Short communication

Quantitative contribution of resistance sources of components to stack performance for solid oxide electrolysis cells

Yifeng Zheng, Qingshan Li, Tao Chen, Cheng Xu*, Wei Guo Wang**

Ningbo Institute of Material Technology & Engineering, Chinese Academy of Sciences, 1219 Zhongguan West Road, Ningbo 315201, PR China

HIGHLIGHTS

- The resistance sources of the components in SOEC stack were quantitatively measured.
- Cell ASR was the main factor that influenced the SOEC stack performance.
- Increasing cell ASR was the main reason for SOEC stack degradation.
- Air electrode CR and hydrogen electrode CR were other reasons for stack degradation.

ARTICLE INFO

Keywords:
Solid oxide electrolysis cell
Stack
Area specific resistance
Interfacial contact

ABSTRACT

Quantitative investigation is conducted on the resistance sources of the components in the NiO–YSZ/YSZ/GDC/LSCF–GDC solid oxide electrolysis cell (SOEC) stack at the H_2O/H_2 ratios of 70/30, 80/20 and 90/10 at 750 °C. The results indicate that the cell resistance accounts for 76.3–66.7% of that of the stack repeating unit (SRU), the contact resistance (CR) between the air electrode current-collecting layer (AECCL) and the interconnect accounts for 23.6–27.0%, the CR between the hydrogen electrode current-collecting layer (HECCL) and the interconnect only accounts for 2.3–3.2%, and the resistance of the interconnect can be neglected. Duration test of the stack is conducted at 0.8 A cm^{-2} for 380 h, the cell resistance increase is found to be the major contribution of the SRU degradation (82.2% of the SRU degradation) while the air electrode CR increase and the hydrogen electrode CR increase are other two important factors.

1. Introduction

In recent years, solid oxide cell (SOC) technology has attracted increasing attention for development of a highly-efficient energy conversion and storage system because it can perform the dual functions of a solid oxide fuel cell (SOFC) and solid oxide electrolysis cell (SOEC) [1,2]. Although the overall SOEC reaction for hydrogen production is simply the reverse of the SOFC reaction for power generation, there are fundamental differences in two operating modes, such as the electric potential, heat flow, mass flux and gas environments, which lead to different performances and system efficiencies in the two operating modes [3]. Therefore, research on SOEC is rather independent from research on SOFC.

For commercial purposes to obtain applicable hydrogen/gas fuel, multiple unit cells with limited voltage need to be connected in series to form a SOEC stack. And from the view of commercialization, long-term stability of the SOEC stack is a premise besides the high hydrogen productivity. A limited number of studies have been performed on the performance and durability issues of SOEC stacks. Significant performance degradation was observed in the large-scale production of hydrogen from nuclear energy using externally manifolded stacks with three modules based on electrolyte-supported cells [4]. A long-term performance degradation of >5% kh^{-1} was also found during durability tests of short stacks based on standard Ni-YSZ supported cells at 800 °C with a current density of 0.5 A cm^{-2} for 2700 h in SOEC mode [5]. These reported degradation rates were much higher than the degradation rates for SOFC stacks.

In previous SOEC stack tests, Cr vapor poisoning, air electrode delamination, microstructure degradation, and seal leakage were found to significantly affect the durability of the stack [6–9]. However, the dominating mechanism for SOEC stack degradation

* Corresponding author. Tel.: +86 574 8668 5139.
** Corresponding author. Tel.: +86 574 8791 1363.
E-mail addresses: xucheng@nimte.ac.cn (C. Xu), wgwang@nimte.ac.cn (W.G. Wang).

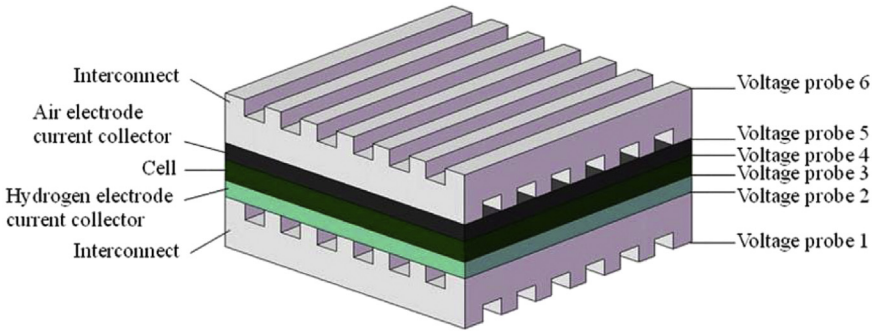

Fig. 1. Schematic diagram of voltage leads on various locations in the SRU.

is not clear yet. Since a SOEC undergoes essentially the reverse process of a SOFC, the SOEC technology can be built based on the extensively researched SOFC technology. In SOFC stacks, the key causes influencing the operating stability of the stacks include stack components and the interfacial contact between the components [10,11]. In previous investigation, our group gave a quantitative description of the contributions of the resistance sources of components to SOFC stack performance [12], and found the increase of the cell resistance is the main reason causing the stack degradation and the anodic contact is also an influencing factor that cannot be neglected during stable operation.

The effect of the interfacial contact to the SOEC stack performance has not been reported yet, especially the variation of the interfacial contact resistance (CR) during long-term operation of the SOEC stack. The present study was thus initiated to give a quantitative investigation on the resistance sources of the SOEC stack with a focus on the contribution of interface contact between different stack components during long-term operation. The SOEC stacks based on hydrogen electrolyte supported NiO–YSZ/YSZ/GDC/LSCF–GDC cells were assembled and the resistance of each stack component was carefully measured. A quantitative analysis was carried out based on the patterns by which the resistance of every component influences the SOEC stack performance.

2. Experimental

The unit cell (UC) used in the experiments was a hydrogen electrode-supported NiO–YSZ/YSZ/GDC/LSCF–GDC (GDC: $Ce_{0.9}Gd_{0.1}O_{1.95}$; LSCF: $La_{0.6}Sr_{0.4}Co_{0.2}Fe_{0.8}O_{3-\delta}$) SOEC cell. Details of the cell manufacturing process and the parameters were reported in our previous research [13]. The cell size in the stack was 10 cm × 10 cm with an active area of about 63 cm^2. For the complete contact between the cell electrodes and the metal interconnects, a coating of NiO current-collecting layer with 80 μm thickness was screen printed on the cell hydrogen electrode and a

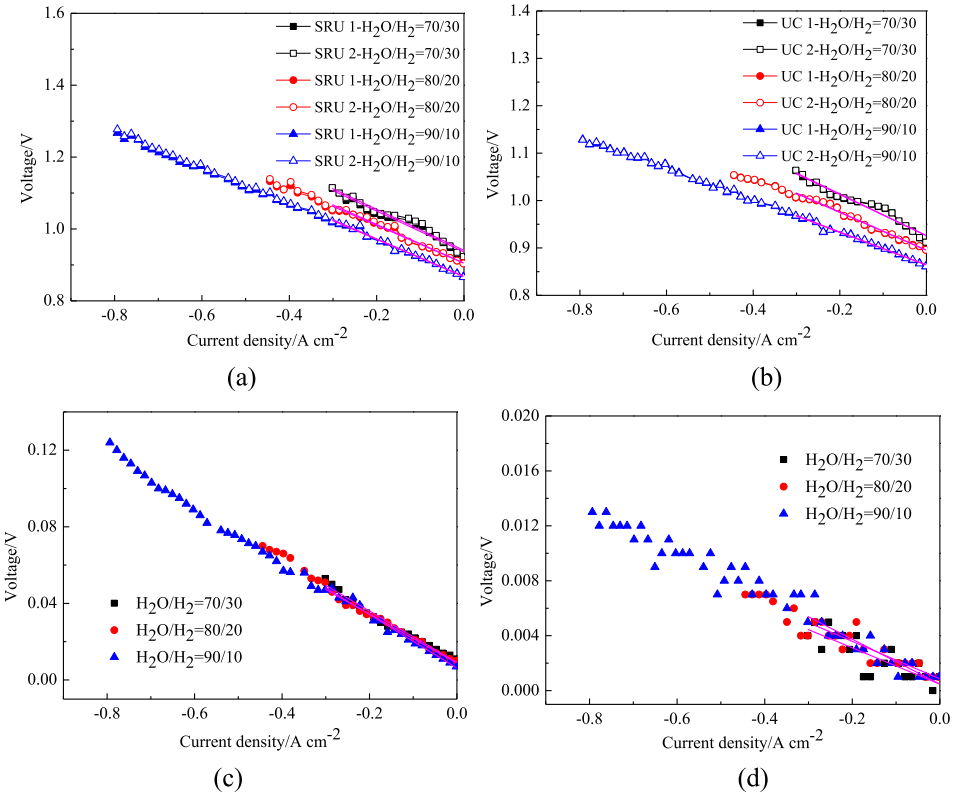

Fig. 2. I–V curves of (a) the SRUs and (b) the UCs under different H_2O/H_2 ratios; voltage rise of (c) air electrode contact and (d) hydrogen electrode contact of the SRU 1#.

Table 1
ASR of the stack components at the beginning and the end of I–V charge.

	H_2O/H_2	SRU/Ω cm^2	UC/Ω cm^2	Air electrode contact/Ω cm^2	Hydrogen electrode contact/Ω cm^2
SRU 1#	70/30	0.569(2)	0.434(3)	0.1342(5)	0.0132(4)
	80/20	0.527(3)	0.399(2)	0.1380(6)	0.0137(5)
	90/10	0.517(4)	0.345(3)	0.1398(6)	0.0163(6)
SRU 2#	70/30	0.570(3)	0.435(3)	0.1345(5)	0.0133(5)
	80/20	0.532(3)	0.403(3)	0.1385(5)	0.0139(5)
	90/10	0.522(3)	0.348(4)	0.1402(6)	0.0160(4)

coating of LSCF current-collecting layer of 80 μm-thick was screen printed on the cell air electrode.

The cells and interconnect plates were then assembled into a 2-cell stack using Al_2O_3–SiO_2–CaO-based glass sealants. The SUS430 ferritic stainless steel was used to create metal interconnects, which were also adopted as co-flow gas channels. To protect from high-temperature oxidation and Cr vaporization, the air electrode side of the interconnect was densely coated with Ni–Cr/LSM composite coating by plasma spraying. The 2-cell stack thus included two pieces of stack repeating units (SRUs): each piece of SRU was consisted of a piece of UC and two pieces of neighboring interconnects as shown in Fig. 1. The SRUs in the stack were numbered 1# and 2#, respectively.

After assembly, the stack was placed into a furnace and heated to 850 °C a a rate of 1 °C min^{-1}. For stack sealing, an external pressure of ~10 N cm^{-2} was loaded on the stack at 850 °C. After remained at 850 °C for 2 h, the stack was cooled to 750 °C for testing. The hydrogen electrode of the stack was subjected to nitrogen purging for 5 min, and then hydrogen and air were fed into the hydrogen and air electrodes of the stack, respectively. After 3 h for hydrogen electrode reduction, the mixture of H_2O/H_2 was then fed to the hydrogen electrode side of the stack and the real-time variation of current and voltage were recorded. After finishing all the tests, the stack was cooled to room temperature at a rate of 1 °C min^{-1} with hydrogen to protect the hydrogen electrode from oxidization. Microstructures of the stack components were examined using a Hitachi S-4800 scanning electron microscope.

Voltage leads were led from the components of the stack as shown in Fig. 1 to quantitatively measure the resistance of the components in the SRUs [12,14]. The interconnect resistance was measured by leads 1–2; the contact resistance between the hydrogen electrode current-collecting layer (HECCL) and the interconnect (hydrogen electrode CR), was measured by leads 2–3; the internal resistance of the UC was measured by leads 3–4; the contact resistance between the air electrode current-collecting layer (AECCL) and the interconnect (air electrode CR), was measured by leads 4–5; and the resistance of the SUR was measured by leads 1–5 [12,15].

3. Results and discussion

3.1. Quantitative contribution of resistance sources to stack electrolysis performance

Fig. 2a and b shows the performance of the SRUs and UCs under different H_2O/H_2 ratios, respectively. It indicated that under the same operating condition, the I–V curves of SRU 1# and SRU 2#, UC 1# and UC 2# were very close. The resistance of SRU 1#, SRU 2#, UC 1# and UC 2# under different H_2O/H_2 ratios was obtained by linear fitting of I–V curves (from 0 A cm^{-2} to 0.30 A cm^{-2}) and the results are listed in Table 1. Apparently, the SRU 1# and SRU 2# were almost consistent, with the increase of the H_2O/H_2 ratio, the ASR of both the SRU and UC decreased significantly whereas the

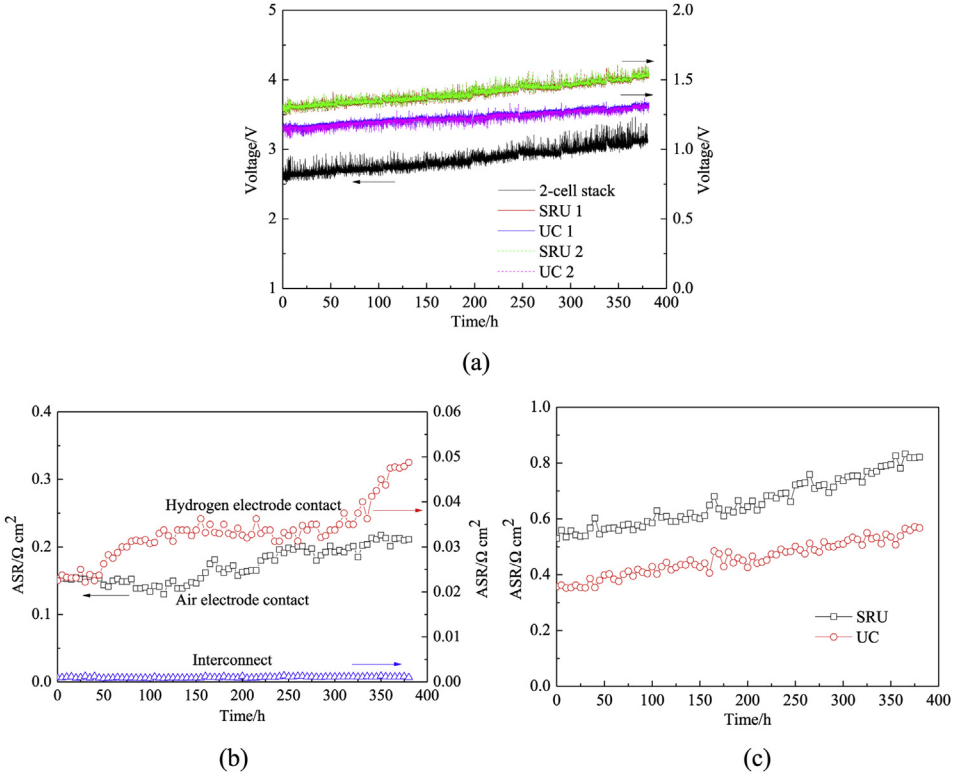

Fig. 3. (a) V-t curves of the stack, the SRUs and UCs at 0.8 A cm^{-2}; ASR of the components in the SRU 1#: (b) air electrode contact, hydrogen electrode contact and the interconnect and (c) the SRU and the UC.

Table 2
ASR of the stack components before and after operation.

Operation time	SRU 1#		SRU 2#	
	0 h	380 h	0 h	380 h
Air electrode contact/Ω cm^2	0.154(2)	0.211(3)	0.157(3)	0.216(2)
Hydrogen electrode contact/Ω cm^2	0.0225(3)	0.0488(4)	0.0227(5)	0.0492(4)
Interconnect/Ω cm^2	0.001(2)	0.001(2)	0.001(2)	0.001(2)
UC/Ω cm^2	0.357(3)	0.568(2)	0.360(3)	0.573(4)
SRU/Ω cm^2	0.530(1)	0.821(3)	0.532(2)	0.825(3)

contribution of the UC to the SRU in ASR decreased. This is because the electrical splitting of water was stimulated by a high steam flow rate due to enhanced gas diffusion through the electrode [16] whereas the interface contact may deteriorate with the increasing steam content.

In the stack, the air electrode CR was measured by the voltage leads 4–5, the hydrogen electrode CR by leads 2–3, and the interconnect resistance by leads 1–2. Because the ASR values of the air electrode contact, hydrogen electrode contact and interconnect were small, the voltage between both ends of the air electrode contact was thus obtained by the difference between the voltage values of the leads 3–4 and leads 3–5, and the voltage between both ends of the hydrogen electrode contact was obtained by the difference between the voltage values of the leads 3–4 and leads 2–4. Therefore, the I–V curves for the air electrode contact and the hydrogen electrode contact could be obtained, as shown in Fig. 2c and d. The ASRs for the air electrode and hydrogen electrode contact could be calculated by linear fitting and the results are listed in Table 1. The results indicated that the hydrogen electrode CR was almost ten times smaller than that of air electrode. With the increase of the H_2O/H_2 ratio, the air electrode CR of the SRU increased, while the hydrogen electrode CR increased slightly. Closer examination of the results showed the air electrode CRs accounted for 23.6%, 26.2% and 27.0%, respectively, while the hydrogen electrode CRs accounted for only 2.3%, 2.6% and 3.2%, respectively. The total resistance of the UC, the air electrode contact and the hydrogen electrode contact was over or less than 100% of SRU due to the test errors of the apparatus. Generally, the UC in the SRU was the main factor determining the performance, accounting for 76.3–66.7%. And the air electrode contact was the second factor, generally accounting for 23.6–27.0%. The hydrogen electrode contact was the minimum factor, only accounting for 2.3–3.2%.

3.2. Quantitative contribution of resistance sources to stack electrolysis durability

Durability test of the SOEC stack under a constant electrolysis current density of 0.8 A cm^{-2} was conducted up to 400 h. The mixture of hydrogen and steam with H_2O/H_2 = 90/10 was introduced to the hydrogen electrode. The variation voltage curves of the stack, SRU 1#, SRU 2#, UC 1# and UC 2# with time are shown in Fig. 3a. It indicated that the degradation rate of the stack reached 4.3%/100 h within 380 h, and the variation voltage curves of the SRU 1# and SRU 2# were almost consistent. The degradation rate of the SRUs reached 4.5%/100 h, and that of the corresponding UCs was

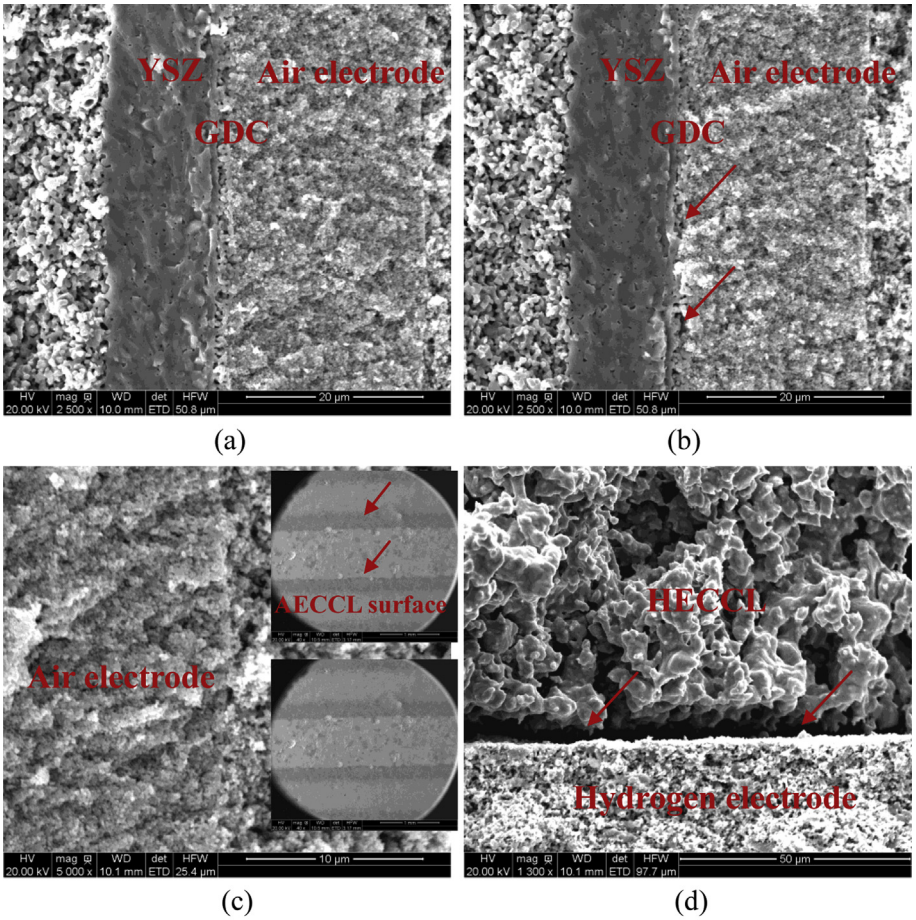

Fig. 4. Cross section morphology of cell (a) before and (b) after electrolysis operation; cross section morphology (c) with surface morphology of the AECCL and (d) of the HECCL on the UC after electrolysis operation.

3.7%/100 h. The degradation of the UC accounted for 82.2% of that of the SRU. The results for the SRU#1 and SRU#2 before and after electrolysis are summarized in Table 2.

Fig. 3b and c shows the variations of the ASRs of the UC, air electrode contact, hydrogen electrode contact and interconnect with time where the ASRs were measured and calculated via voltage measurements [12,15]. The air electrode CR slightly dropped within 115 h, and then continuously increased, the hydrogen electrode CR and the UC resistance continuously increased with time, and the interconnect resistance remained unchanged and negligible (0.001 Ω cm^2). The resistance of the UC rose by 59.1%, the air electrode CR rose by 37.0% and the hydrogen electrode CR rose by 116.9%. These three sources contributed to the degradation of the SRU, which had a resistance increase by 55%. Among these three factors, the UC resistance increase was the main reason leading to the degradation of the SRU.

Microstructures of the stack components were examined using SEM. Fig. 4a and b illustrate the cross-section images of the cell before and after electrolysis operation. The microstructure of the UC exhibited minimal change after electrolysis operation except parts of the LSFC-GDC air electrode delamination from the GDC, which could be the main factor that caused the cell degradation. Fig. 4c shows the cross section morphology and surface morphology of the AECCL on the UC after electrolysis operation. It can be seen that the AECCL was combined well with the cell, while the contact traces left by the metal interconnect on the AECCL surface were vague (the inserted figure), indicating weak contact between the metal interconnect and the AECCL. The weak contact may deteriorate during operation, which results in increasing the air electrode CR with increase of the operation time. Fig. 4d shows the cross section morphology of the HECCL on the UC after electrolysis operation. The agglomeration of Ni particles in the HECCL and delamination of the HECCL by the hydrogen electrode of the cell can be observed. The agglomeration of Ni particles could cause the decrease of the conductivity during the stack operation [17], and the delamination of HECCL could cause the decrease of electron conduction in the stack. Both could result in the continuously increase of the hydrogen electrode CR.

4. Conclusions

The quantitative contribution of resistance sources of components to the stack performance was investigated in a NiO–YSZ/YSZ/GDC/LSCF–GDC SOEC stack at 750 °C. The results indicated that during instantaneous I–V testing the UC was the main factor that influenced the stack performance, the air electrode CR was the second factor that influenced the stack performance, and the hydrogen electrode CR was the third factor that influenced the stack performance, while the resistance of the interconnect was small and could be neglected. When the durability of the stack was conducted under a constant electrolysis current density of 0.8 A cm^{-2} for 380 h, the increasing resistance of the UC was the main reason for the degradation of the SRU, and the air electrode CR was another important factor that influenced the stack degradation. In addition, the hydrogen electrode CR was also an innegligible factor that influenced the stack degradation.

Acknowledgments

This work was supported by the Ningbo Natural Science Foundation (2013A610028) and China Postdoctoral Science Foundation (2012M521208).

References

[1] S.I. Lee, J. Kim, J.W. Son, J.H. Lee, B.K. Kim, H.J. Je, H.W. Lee, H. Song, K.J. Yoon, J. Power Sources 250 (2014) 15–20.
[2] G.B. Jung, J.Y. Chen, C.Y. Lin, S.Y. Sun, Int. J. Hydrog. Energy 37 (2012) 15801–15807.
[3] M.A. Laguna-Bercero, J. Power Sources 203 (2012) 4–16.
[4] C.M. Stoots, J.E. O'Brien, K.G. Condie, J.J. Hartvigsen, Int. J. Hydrog. Energy 35 (2010) 4861–4870.
[5] M. Petitjean, M. Reytier, A. Chatroux, L. Bruguiere, A. Mansuy, H. Sassoulas, S.D. Iorio, B. Morel, J. Mougin, ECS Trans. 35 (2011) 2905–2913.
[6] Y. Matsuzaki, I. Yasuda, Solid State Ionics 132 (2000) 271–278.
[7] K.F. Chen, S.P. Jiang, Int. J. Hydrog. Energy 36 (2011) 10541–10549.
[8] V.I. Sharma, B. Yildiz, J. Electrochem. Soc. 157 (2010) B441–B448.
[9] X.Y. Zhang, J.E. O'Brien, R.C. O'Brien, J.J. Hartvigsen, G. Tao, G.K. Housley, Int. J. Hydrog. Energy 38 (2013) 20–28.
[10] H.T. Lim, A.V. Virkar, J. Power Sources 185 (2008) 790–800.
[11] L. Barelli, E. Barluzzi, G. Bidini, Int. J. Hydrog. Energy 38 (2013) 5060–5074.
[12] L. Jin, W.B. Guan, X. Ma, H.J. Zhai, W.G. Wang, J. Power Sources 253 (2014) 305–314.
[13] W. Wu, W.B. Guan, G.L. Wang, F. Wang, W.G. Wang, Advanced Energy Mater. 4 (2014), http://dx.doi.org/10.1002/aenm.201400120.
[14] W.B. Guan, L. Jin, W. Wu, Y.F. Zheng, G.L. Wang, W.G. Wang, J. Power Sources 245 (2014) 119–128.
[15] X.Y. Zhang, J.E. O'Brien, R.C. O'Brien, G.K. Housley, J. Power Sources 242 (2013) 566–574.
[16] S.D. Kim, J.H. Yu, D.W. Seo, I.S. Han, S.K. Woo, Int. J. Hydrog. Energy 37 (2012) 78–83.
[17] D. Simwonis, F. Tietz, D. Stöver, Solid State Ionics 132 (2000) 241–251.